



## THERMAL BOUNDARY LAYER INSTABILITIES IN VISCIOUS FLUIDS

Anne Davaille <sup>\*,\*\*</sup>, Sophie Androvandi <sup>\*</sup>, Judith Vatteville <sup>\*</sup>, Angela Limare <sup>\*</sup>, Valérie Vidal <sup>\*</sup>, Michael Lebars <sup>\*</sup>

<sup>\*</sup> Institut de Physique du Globe de Paris, France

<sup>\*\*</sup> Laboratoire FAST, CNRS / Univ. P6 / Univ. Psud, Orsay, France

### KEYWORDS:

**Main subject(s):** Thermal convection, boundary layer, instabilities

**Fluid:** sugar syrup

**Visualization method(s):** TLCs, PIV

**Other keywords:** viscous fluid dynamics, mantle convection

### ABSTRACT :

*We study the development of thermal boundary layer instabilities in newtonian fluids whose viscosity depends strongly on temperature. We use PIV and a new technique using liquid crystals slurries illuminated by a laser sheet to determine the velocity and thermal fields in the experimental cell. This allows us to focus on the local properties of the thermal instabilities for Rayleigh numbers  $10^4 \leq Ra \leq 10^8$ , Prandtl numbers  $10^3 \leq Pr \leq 10^6$ , and viscosity ratio across the tank  $3 \leq \gamma \leq 4000$ . The temperature-dependence of viscosity introduces a strong asymmetry in the thermal boundary layers ("TBL"). At high Rayleigh numbers, hot instabilities develop as mushroom-shaped plumes while cold instabilities develop as thin fingers under a stagnant conductive "lid". We further show that the phenomenological model of Howard (1964) describes very well the hot instabilities formation: the TBL first grows by conduction until the local Rayleigh number calculated across it reaches a critical value  $Ra_c$ . Then a plume develops from the TBL. Once the latter has been exhausted, the plume detaches and the TBL is locally rebuilt by heat conduction, starting a new cycle. By comparison, cold more viscous instabilities only disappear by merging.*

## 1. Introduction:

Thermal convection in viscous fluids is a common occurrence both in industry (e.g. chemical reactors) and nature (e.g. lava lakes, magma chambers, and mantle). Besides, Rayleigh-Bénard convection in a shallow cavity heated from below is a classic example of a non-linear system exhibiting a sequence of transitions towards chaos as a control parameter increases. But convective phenomena are so rich and diverse that despite numerous studies (see [1,2] for recent reviews), it is still only partially understood.

Geological fluids encountered in natural systems such as lava lakes or planetary mantles have a viscosity which depends strongly on temperature. Convection therefore is characterized by three dimensionless numbers [3-5]:

.the Rayleigh number, ratio of the driving thermal buoyancy forces to the resisting effects of thermal diffusion and viscous dissipation:

$$Ra = \frac{\alpha g \Delta T d^3}{\kappa \nu_2} \quad (1),$$

where  $d$  is the total fluid depth,  $\Delta T$  is the temperature difference applied across it,  $g$  is the gravitational acceleration,  $\alpha$  is the thermal expansivity,  $\kappa$  is the thermal diffusivity and  $\nu_2$  is the kinematic viscosity of the fluid at its bottom hot boundary temperature  $T_2$ .

.the Prandtl number, which compares the heat and vorticity diffusivities

$$Pr = \nu_i / \kappa \quad (2).$$

.the viscosity ratio across the fluid layer:

$$\gamma = \nu_1 / \nu_2 \quad (3),$$

where  $\nu_1$  is the kinematic viscosity of the fluid at its top cold boundary temperature  $T_1$ .

We focus here on the regime at high Rayleigh number ( $>10^6$ ) and high  $Pr$  ( $>10^3$ ), where convective motions are chaotic and take the form of thermal plumes [6]. Of particular interest is the development of plumes as transient instabilities of a (TBL) thermal boundary layer [7-9]. Howard [10] developed a phenomenological model for plume formation, and gave scalings for the onset time of thermal instabilities and the boundary heat flux which agree well with experimental data [7, 5, 11]. But the detailed sequence of local plume formation and disappearance has not yet been studied, due to experimental and numerical limitations.

In particular, to reach  $Ra$  between  $10^3$  and  $10^8$ , temperature differences between 10 and 70°C have to be imposed across the experimental cell. Moreover, convective motions are slow (1 mm/sec to 1 mm/hour), temperature heterogeneities can reach 10-25°C, and experiments can run for several weeks. To monitor the experimental temperature field on such scales, we have developed a new technique using thermochromic liquid crystals (TLC) slurries which enables to image several “isotherms” with a precision of  $\pm 0.1^\circ\text{C}$ , or 0.2 to 1% of the typical temperature differences applied to the system. In certain cases, local temperature gradients are available as well. This technique was used in combination with PIV to obtain simultaneously the velocity field.

In section 2, we present the experimental set up and the calibration procedures. In section 3, we use our new method to describe the pattern of thermal convection, and the onset of thermal boundary layer instabilities, in viscous homogeneous fluids with a temperature-dependent viscosity.

## 2 Set up and visualization techniques

### 2.1 Experimental set up

The experimental set up is presented on fig.1. The convection cell is a rectangular plexiglas tank with typical horizontal extent between 30 and 40 cm, and height between 4 and 20 cm. Its top and bottom boundaries are copper plates, the temperatures of which are regulated by thermostated circulating fluids (water and alcohol). The top and bottom temperatures are therefore kept constant and uniform to within  $0.05^{\circ}\text{C}$ . Thermocouples embedded within the copper plates allow to measure their temperature through time. All the sides are covered with styrafoam to minimize heat losses. The whole system is carefully levelled.

The experimental fluid is a sugar syrup (GS6075 from Syral), whose viscosity depends strongly on temperature and typically ranges between 0.1 and  $10^4$  Pa.s (fig.2). Its physical properties were measured, save the heat capacity, and are given in Table 1.

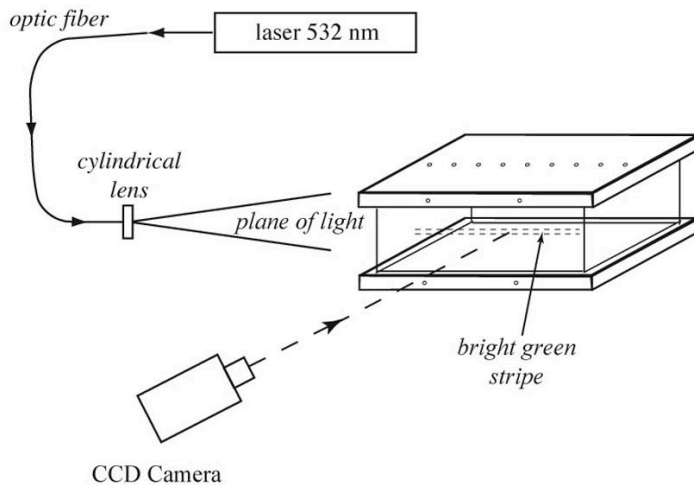


Fig.1: Experimental set up

Cross-sections of the tank were illuminated with a laser sheet. We used a compact solid-state diode-pumped, frequency doubled Nd :Vanadate ( $\text{Nd}:\text{YVO}_4$ ) laser, emitting a single-frequency green at 532 nm, with power from 0.01 up to 2W. The laser beam is expanded by a cylindrical divergent lens before entering the experimental tank (fig.1). The images are taken at  $90^{\circ}$  from the laser sheet with a digital camera (Canon 8.2 Mpixels) or with a black and white CCD (LaVision 1280x1020 pixels). They are corrected for optical deformation by calibration on a grid.

The fluid was seeded with glass particles ( $10\mu\text{m}$ -diameter) to visualize velocity fields. Images were taken using the CCD black and white camera every second (exposure time = 100 ms). Velocity fields were calculated using the PIV package Davis 6 by LaVision.



Property	Sugar syrup
$\eta$ (20°C)	6.00 (Pa.s)
k	0.3865 (J/m/s/K)
$C_p$	1460 (J/kg/K)
$\rho$ (20°C)	1388 (kg/m <sup>3</sup> )
$\alpha$	$5.74 \times 10^{-4}$ (°K <sup>-1</sup> )

Table 1: Physical properties of the fluids:  $\eta$ , viscosity; k, heat conductivity;  $C_p$ , heat capacity;  $\rho$ , density;  $\alpha$ , thermal expansion.

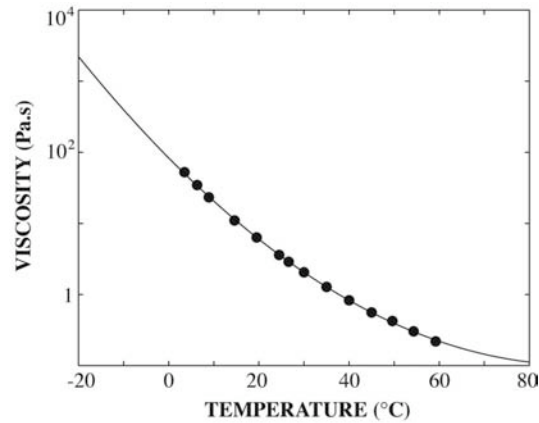


Fig.2: Sugar syrup viscosity as a function of temperature mesurée par RS 600 (ThermoRheo).

## 2.2 Temperature field: TLCs and “isotherms”

The use of thermochromic liquid crystals has allowed to visualize the temperature field on a 2D-plane in the fluid flow without its perturbing [12]. It was first used as paint on a surface to determine qualitatively the convective pattern [13]. Then it became possible to mix the TLC slurry directly within the fluid and to illuminate the tank cell on cross-sections (fig.1). One of the main applications of this technique has been the study of aqueous turbulent flows (e.g.[14-17]). The use of this method to quantitatively measure the temperature field needs a high precision colour CCD camera and a very precise calibration of the colour of the liquid crystals particles against the true temperature. Moreover, the total temperature range accessible with one particular TLC slurry is usually around 2-3 °C. This technique has lately been further extended to the joint measurement of temperature and velocity in a three dimensional field [18-19]. An uncertainty analysis performed by Fujisawa & Hashizume [21] gives an error less than 0.1°C, or 5% of the total temperature difference imposed to the system, for a calibration method based on a hue-saturation-intensity approach.

Here, given the large temperature differences encountered (10-70°C), we choose to visualize only several “isotherms”, but with good precision (0.1°C, i.e. 0.2 to 1% of the total temperature difference). The flow was seeded with 40  $\mu$ m diameter thin-walled encapsulated (custom made) chiral nematics liquid crystals from Hallcrest (Table 1). These slurries are miscible in all proportions in aqueous solutions. Since typical experiments run for several days, micro-encapsulated TLC were preferred to pure TLC which, although brighter, degrade faster when in solution. Four different temperature-sensitive liquid slurries were introduced and mixed in the experimental fluid, in the proportion of 0.1g/L each. Given the large viscosity of the working fluid, there is no differential motion between the TLC and the fluid on the duration of an experiment. Moreover, the characteristic thermal diffusion time through the capsules is about 10ms. Given the typical velocities (mm/s) and thermal gradients in the experimental tank, this ensures that TLCs’ state is at equilibrium with the surrounding fluid temperature. In order to visualize a single « isotherm », i.e. a temperature range as narrow as possible, the solution is illuminated with a laser sheet.

## 2.3 Calibration procedure of the “isotherms”

Since the accuracy of TLC temperature measurements is strongly influenced by the viewing angle [20] and the nature of the fluid, a calibration is performed each time the experimental fluid is changed, and with the experimental set up used for the convection experiments. Two different methods were used to find the precise temperature interval for which each liquid crystal brightens at 532 nm wavelength.

2.3.1 Steady state calibration

A vertical stable temperature gradient is applied to the experimental tank (fig.3). It establishes itself by conduction from the copper plates in a characteristic time  $t=d^2/k$  around 44 hours, and we always waited more than three days before beginning the calibration procedure. Temperature measurements within the tank are performed with a vertical thermocouple probe that can be placed on different locations through holes in the upper plate. This probe contains 14 calibrated thermocouples of E-type located at 14 fixed depths, which allow to follow the vertical temperature profile through time with a 0.05°C precision.

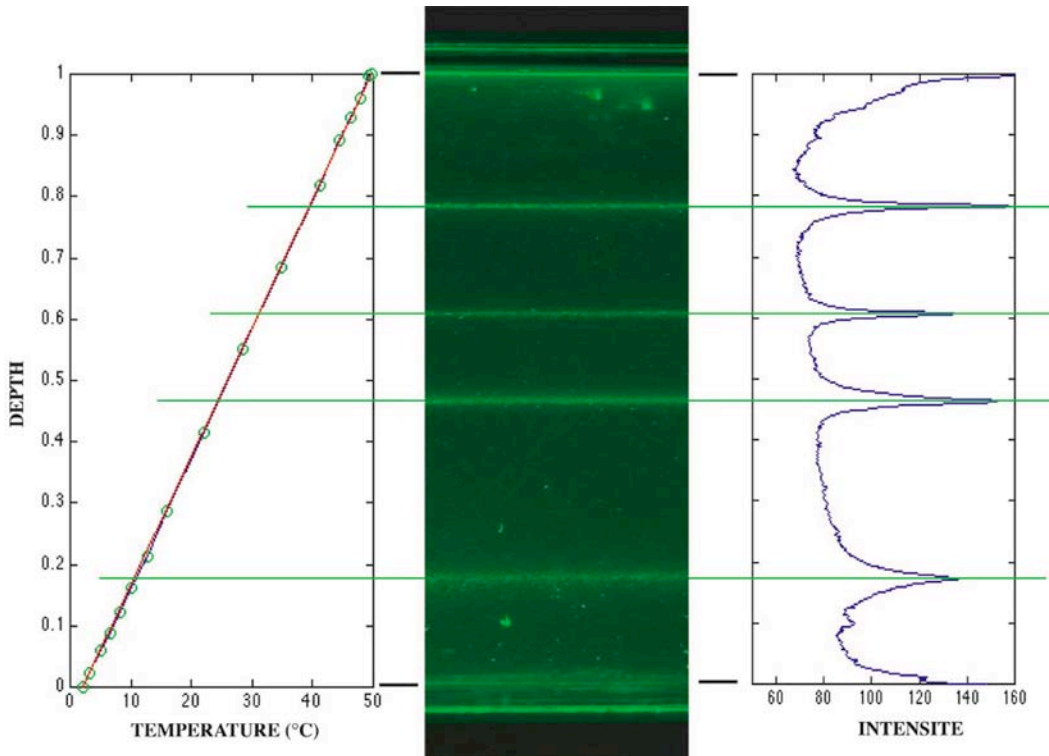


Fig.3: Steady-state calibration. Left) Temperature measured by the thermocouples (circles) as a function of the normalized depth. Middle) photograph taken with the digital camera. The isotherms appear as bright lines. Left) Horizontally averaged light intensity as a function of depth.

Fig.3 shows an example of the picture obtained when applying a bottom temperature of 2.20°C and a top temperature of 49.65°C. Each slurry brightens over a different temperature subrange and therefore generates a horizontal bright green line: for this 47.45°C temperature difference, four distinct stripes are visible. Each stripe presents a finite thickness: although each TLC responds at a given wavelength to a precise temperature, the polymeric capsules enclosing them introduce a scatter around

this value. On a plot of the intensity as a function of depth, or temperature, each stripe corresponds therefore to a peak whose maximum defines the value of the « isotherm », and whose thickness gives a measure of the local temperature gradient (fig.3c). The peaks were symmetric around their maximum value for all four slurries. If we define the value of an “isotherm” as the peak value of the stripe, the uncertainty on the absolute temperature of the isotherm is  $\pm 0.10^\circ\text{C}$ . This takes into account all the contributions due to height and true vertical temperature profile determination. The temperature difference across a stripe is defined as the full width at half maximum of the light intensity. It ranges between  $0.50^\circ\text{C}$  (40C2W) and  $1.20^\circ\text{C}$  (10C2W) (table 2).

Product name	BM/10C2W/S40 « A »	BM/24C2W/S40 « B »	BM/31C2W/S40 « C »	BM/40C2W/S40 « D »
Red Start - Blue Start	10.2 - 12.3 °C	24.3 – 26.5 °C	31.0 – 33.2 °C	40.1 – 42.2 °C
<b>Steady-state</b>				
Peak value	10.70 °C	24.35 °C	31.10 °C	39.50 °C
Half-width	-0.60 °C +0.60 °C	-0.30 °C +0.30 °C	-0.25 °C +0.25 °C	-0.25 °C +0.25 °C
<b>Step calibration</b>				
Peak value		24.35 °C	31.10 °C	39.50 °C
Half-width		-0.30 °C +0.30 °C	-0.25 °C +0.25 °C	-0.25 °C +0.25 °C

Table 2: Calibrated values of the “isotherms” and their width for both calibrations. The range of temperature to which each TLCs slurry is sensitive (Red start to Blue start) is given by the constructor with a  $\pm 0.5^\circ\text{C}$  tolerance).

### 2.3.2 Time-dependent calibration

The calibration values found above were further checked by applying a temperature quasi-step to the fluid initially at ambient uniform temperature (fig.4a). In that case, an analytical solution for the temperature history within the tank exists [21], which predicts well the temperature signals registered by the thermocouple probe (fig.4a). One can then follow the progression through time of the different stripes through the tank (fig.5a), and compare the data to the temperature prediction (fig.4b). The best fit between the data (stripe evolution) and the analytical solution defines the value of the isotherm. This method gives the same values as the steady-state calibration (Table 2). Moreover, the thickness of each stripe is seen to increase through time, in agreement with the smoothing of the temperature gradients within the tank as time increases (fig.5b). It proves that the corresponding temperature difference across each stripe does not change. The half width of each stripe is therefore a reliable measurement of the local temperature gradient.

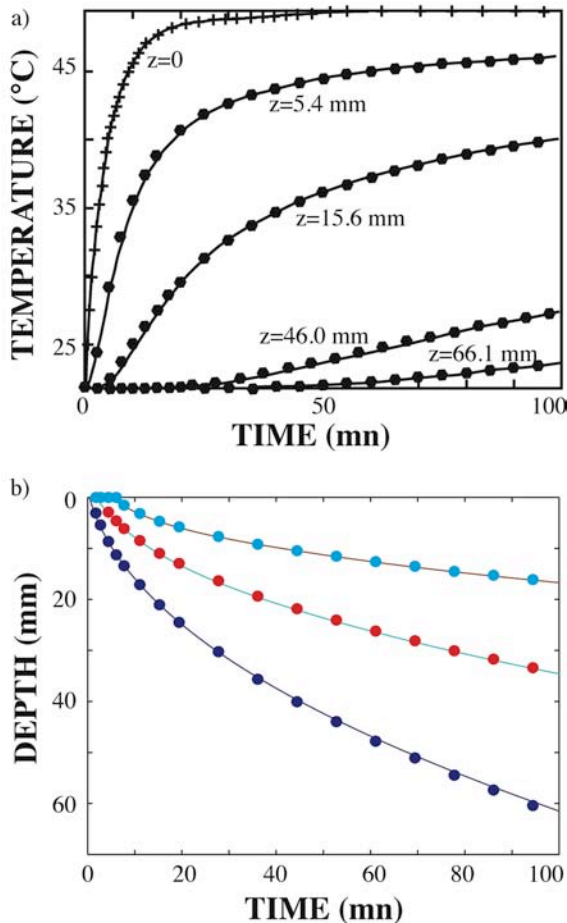


Fig.4: a) Evolution of the temperature measured by the thermocouples during the time-dependent calibration. The depth of each thermocouple is indicated in mm. Cross and hexagons indicate the measurements while the lines correspond to the analytical solution. b) Depth of the isotherms through time. The dots corresponds to the measurements of the three intensity peaks of fig.5, while the lines correspond to the analytic solution for  $T=24.35^{\circ}\text{C}$  (bottom curve),  $T=31.10^{\circ}\text{C}$  and  $T=39.50^{\circ}\text{C}$  (top curve).

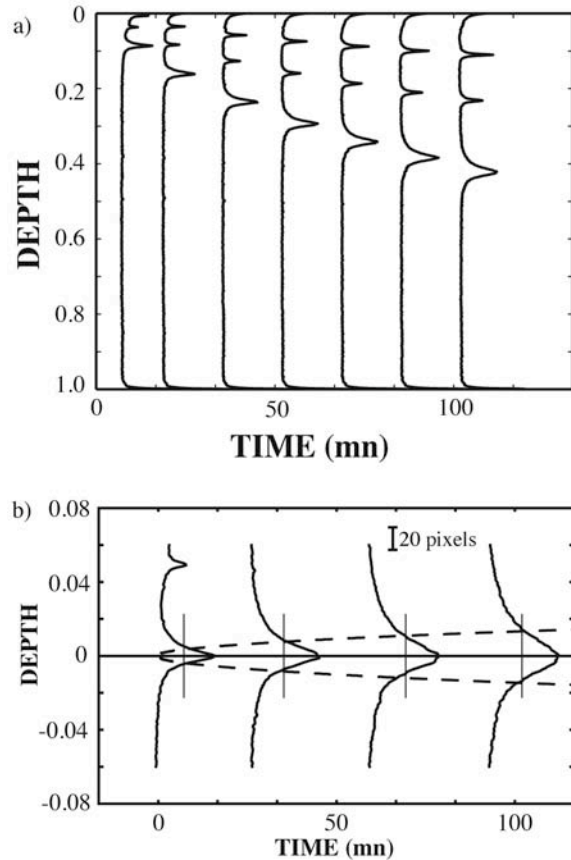


Fig.5: Vertical profiles of the horizontally averaged light intensity (in arbitrary units) for increasing time (to which corresponds each base line). a) Profiles across the whole tank. The bottom peaks correspond to the  $24.35^{\circ}\text{C}$  isotherm, the middle ones to  $31.10^{\circ}\text{C}$  and the top ones to  $39.50^{\circ}\text{C}$ . b) Close-up on the  $24.35^{\circ}\text{C}$  peaks. The peaks have been centered on the maximum intensity value depth at each time. The dashed lines indicate the half-widths ( $+0.3^{\circ}\text{C}$  and  $-0.3^{\circ}\text{C}$ ) predicted by the analytical solution. They predict well the data.

### 3 Convective patterns in viscous fluids at high Rayleigh number

#### 3.1 Development of hot thermal boundary layer instabilities

The sugar layer, initially at uniform temperature  $T_m$ , was suddenly heated from below at a constant temperature  $T_m + \Delta T_m$ . Fig.6 presents the development of the hot convective instabilities. At first, the isotherms (bright lines) remain horizontal and the temperature front moves away from the boundary by conduction (fig.6a): there is no motion in the fluid. Then the conduction layer (or TBL)

contained between the moving front and the outer boundary suddenly becomes unstable (fig.6b) and breaks up (fig.6c). It produces mushroom-shaped plumes (fig. 6c,e,g). The tip of their heads ascends initially with a constant velocity (fig.7), and slows down when it nears the upper boundary. The point of maximum vertical velocity is initially within the head (fig.6d, fig.8), and recedes into the stem as the head slows down (fig.6f,h, fig.8). In this latter stage, the head is fed by the stem as in a plume from a fixed source (e.g. [22,16]). When the plume reaches the top boundary, it spreads under it, forming a large pond (fig.6g). During its ascent, the plume also cools by heat diffusion as indicated by the progressive disappearance of the hottest isotherm (here  $40.5^{\circ}\text{C}$ ) from fig.6c to fig.6g. Meanwhile, the TBL empties itself into the plume (fig.6d,f). Once its entire content has been exhausted, the plume tail starts to disappear from the bottom boundary upwards both on the temperature and on the velocity field (fig.6g-h, fig.8). At the end, only the pond below the top boundary is visible, and is slowly disappearing as the plume is cooling. Meanwhile, the TBL starts to locally build up again by conduction and a new cycle begins.

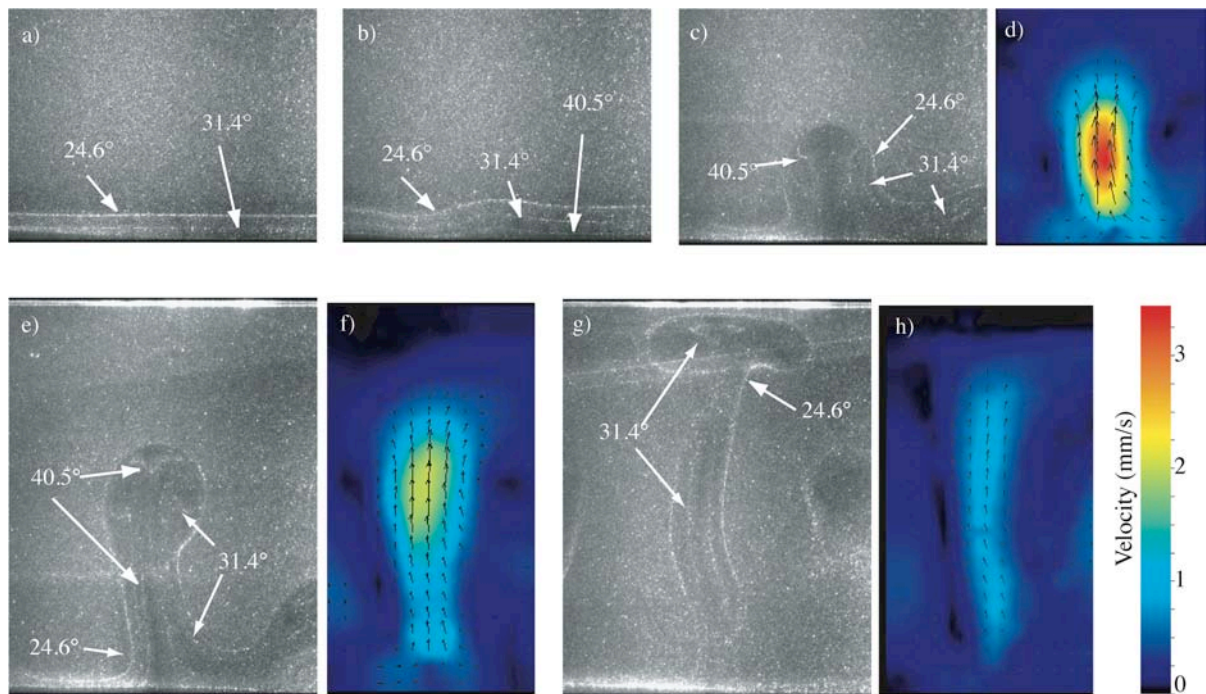


Fig.6: Thermal boundary layer instabilities in a layer of sugar syrup, initially at  $21^{\circ}\text{C}$  and suddenly heated from below at  $53^{\circ}\text{C}$  ( $\text{Ra}=1.7 \times 10^6$ ). a) Picture taken at  $t=300$  s. The isotherms appear as white lines (Their calibrated values differ from table 1, since it is not the same fluid batch). The TBL is growing by conduction from the lower boundary. b)  $t=400$  s. The TBL becomes unstable. c)  $t=460$  s. A thermal plume, outlined by the  $24.6^{\circ}\text{C}$  isotherm rises from the TBL, and the TBL begins to shrink. d) corresponding velocity field deduced from PIV. The colour background represents the velocity magnitude. e)  $t=500$  s. The plume is well developed and the TBL is emptying itself in it. f) corresponding velocity field. g)  $t=600$  s. The plume head has reached the upper boundary and begins to spread under it. The TBL has nearly disappeared and the conduit is disconnected from its source. h) corresponding velocity field.

The longest stage of plume formation is the conductive stage of TBL building (fig.6,7). Both the TBL cycle duration  $\tau$  and the plume lifetime  $\tau_p$  are proportional to the time  $\tau_c$  at which the TBL becomes unstable. Howard [10] suggested that this happens when the thickness  $\delta = \sqrt{\pi \kappa \tau_c}$  of the TBL is such that the local Rayleigh number  $Ra(\delta, \Delta T_m)$  exceeds the critical value  $Ra_c$ , which gives :

$$\tau_c = \frac{H^2}{\pi \kappa} \left( \frac{Ra_c}{Ra_m} \right)^{2/3} \quad (4).$$

Experimental measurements of  $\tau_c$  agree with eq.(4) if  $Ra_c = 1300 \pm 500$  [23]. This value is close to the marginal stability value of 1100 predicted for a linear temperature gradient between rigid and free-slip isothermal boundaries, which are the conditions prevailing across the TBL. Estimating the recurrence time  $\tau$  between two TBL instabilities on fig.6 and 7 as the time of plume detachment, we find  $t = 550s$ , so that the conductive stage occupies 67% (370s) of the whole cycle (fig.7a). Recording the temperature fluctuations in the hot TBL by thermocouples, Sparrow & al [7] and Manga & Weeraratne [5] also found that eq.(4) fitted cyclicity measurements if  $Ra_c = 2050 \pm 300$ . So both methods show that plume recurrence time  $\tau$  scales as plume onset time  $\tau_c$ , albeit about 30% longer.

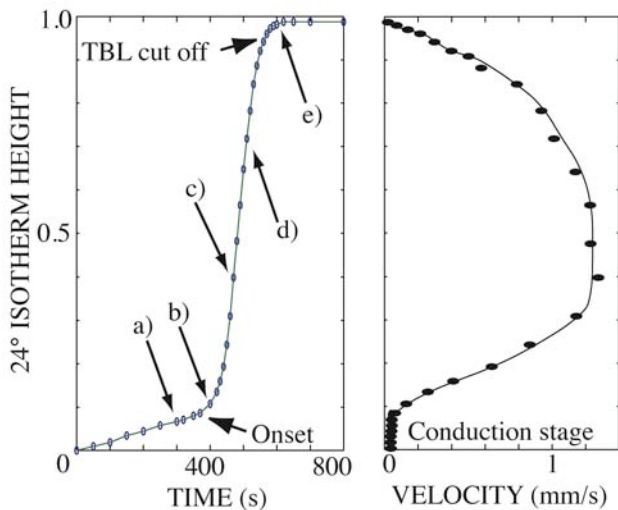


Fig.7 : a) Height (normalized by the tank depth) of the 24.6°C isotherm as a function of time, and b) of the uplift velocity. Convection onset is at  $t = 370$  s. The plume ascent is rapid compared to the conductive stage. The plume becomes detached from the TBL at  $t = 550$  s.

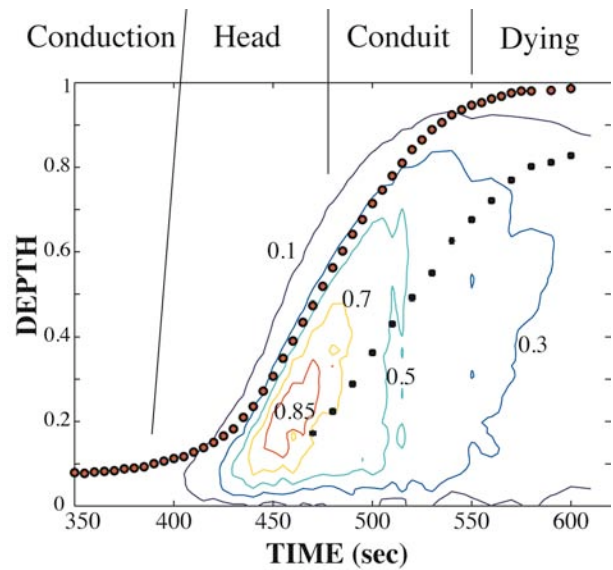


Fig.8 : Vertical velocity along the plume axis as a function of depth and time. The numbers gives the isocontours as fractions of the maximum vertical velocity. The dots shows the top, and the squares the bottom, of the plume head.

Those measurements, as well as the sequence of images described in fig.6, confirms the validity of Howard's phenomenological model to describe qualitatively and quantitatively TBL instabilities [24].

### 3.2 Morphology in well-developed convection

The syrup layer is now heated from below and cooled from above at constant temperature and both cold and hot instabilities develop (fig.9). Since sugar syrup viscosity depends strongly on temperature, cold downwellings are more viscous, and hot upwellings are less viscous, than the fluid which they are invading. In the case of compositional plumes, Olson and Singer [22] showed that their morphology was depending on the local viscosity ratio. Fig.9 shows that this is also the case for thermal plumes.

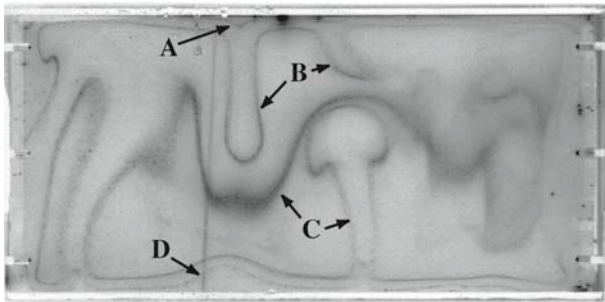


Fig.9: Hot and cold TBL instabilities for sugar syrup cooled from above and heated from below ( $Ra=4.7 \times 10^6$ ). The viscosity contrast between the coldest ( $5.0^\circ\text{C}$ ) and the hottest fluid ( $51.9^\circ\text{C}$ ) is 116. The isotherms (labelled A,B,C,D –see Table 2) appear as black lines since it is a negative of the picture taken with the 8.2 Mpixel Canon digital camera

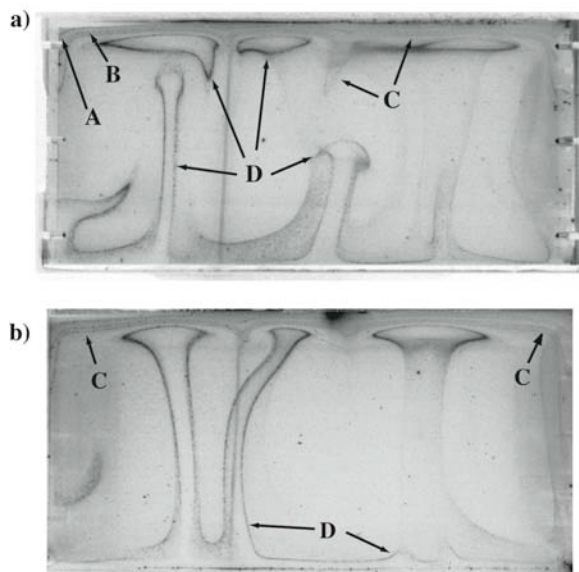


Fig.10: Hot instabilities in sugar syrup cooled from above and heated from below ( $Ra=1.1 \times 10^7$ ). The viscosity ratio between the coldest ( $-16.0^\circ\text{C}$ ) and the hottest fluid ( $52.4^\circ\text{C}$ ) is 3245. a) New hot instabilities will feed the remains of older disconnected ones, b) two plumes are merging by their tails. Fluid at temperature « D » is 2.5 times more viscous than the hot boundary, fluid at « C » is 5.5 times more viscous, and fluid at « B » is 11 times more viscous.

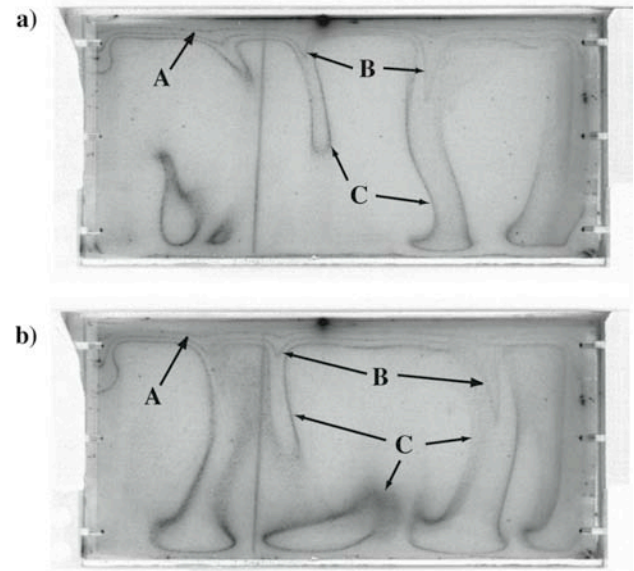


Fig.11: Cold TBL instabilities for sugar syrup cooled from above only ( $Ra=1.2 \times 10^7$ ). The viscosity contrast between the coldest ( $-18^\circ\text{C}$ ) and the hottest fluid ( $38^\circ\text{C}$ ) is 1580. a) Cold diapirs development. b) Merging of two diapirs by their tails. Fluid at temperature « C » is 1.9 times more viscous than the hot interior, fluid at « B » is 3.8 times more viscous, and fluid at « A » is 19 times more viscous.

Hot instabilities are mushroom-shaped, and one can distinguish a plume head and a plume tail (fig.9 and 10). Even long after the convection onset (typically after more than  $50 \tau$ ), they are still transient features. They have two ways of disappearing, either by disconnecting from the hot TBL and fading by thermal diffusion under the cold boundary (fig.6 and fig.10a) or by merging together (fig.10b). Cold instabilities descend as fingers (fig.11a), which buckle, then slowly spread along the bottom boundary. They disappear by plume merging (fig.11b).

When the viscosity contrast across the fluid layer exceeds 500, previous works [3,4,25] have shown that convection was developing below a stagnant lid which was taking most of the viscosity variations. Comparing fig.9 (which  $\gamma=116$ ) and fig.10 (where  $\gamma=3245$ ), we can indeed see that in the latter case, the upper cold TBL becomes much thicker than the lower hot one. Using the syrup viscosity law (fig.2), one can also convert the « isotherms » in « iso-viscosity ratio » between the fluid at the isotherm temperature and the hottest fluid. We then further see that the viscosity ratio between the plumes or diapirs and the bulk interior of the fluid does not exceed  $\sim 10$ , in agreement with previous work.

#### 4 Conclusions:

We have developed a new method, using thermochromic liquid crystals, which allows for visualisation of isotherms (with a precision of  $0.1^\circ\text{C}$ ) and local temperature gradients in a plane illuminated by a laser. Although this technique does not give the complete 2D temperature field, it gives quantitative information, allowing to visualize the development of convective patterns, or measure temperature gradients in thermal boundary layers. It is especially useful in viscous systems where the temperature anomalies are typically greater than  $10^\circ\text{C}$ . It can be combined with PIV to determine simultaneously the velocity field.

We used this technique to study the development of thermal boundary layer instabilities in a viscous fluid. The phenomenological model of Howard [10] is shown to describe well hot instabilities formation. And in a strongly temperature-dependent fluid, hot instabilities develop as mushroom-shaped plumes while cold instabilities develop as thin fingers. Further work is under way to characterize the cold more viscous instabilities.

#### References

1. Bodenschatz E., W. Pesch and G. Ahlers, Recent developments in Rayleigh-Bénard convection, *Annu. Rev. Fluid Mech.* 32 , 709-773, 2000.
2. Davaille A and Limare A. Laboratory Studies in Mantle Convection in *Treatise of Geophysics*, volume editor D. Bercovici, editor G. Schubert, Elsevier, 89-165, 2007.
3. Richter F.M., H.-C. Nataf and S.F. Daly, Heat transfer and horizontally averaged temperature of convection with large viscosity variations, *J. Fluid Mech.* 129, 173-192, 1983.
4. Davaille A. and C. Jaupart, Transient high-Rayleigh number thermal convection with large viscosity variations, *J. Fluid Mech* 253 : 141—166, 1993.
5. Manga M., D. Weeraratne & S.J.S. Morris, Boundary-layer thickness and instabilities in Bénard convection of a liquid with a temperature-dependent viscosity, *Phys. Fluids*, 13, 802-805, 2001.
6. Krishnamurti R., On the transition to turbulent convection. *J.Fluid Mech.* 42 : 295—320, 1970.

7. Sparrow E.M., R.B. Husar and R.J. Goldstein, Observations and other characteristics of thermals. *J Fluid Mech* 41 : 793—800, 1990
8. Trompert R.A. and U. Hansen, On the Rayleigh number dependence of convection with a strongly temperature-dependent viscosity, *Phys. Fluids* 10, 351-360, 1998.
9. Xi H-D, S. Lam and K.-Q. Xia K-Q, From laminar plumes to organized flows : the onset of large-scale circulation in turbulent thermal convection, *J. Fluid Mech.* 503, 47-56, 2004.
10. Howard L.N., Convection at high Rayleigh number. In *Proc. 11th Intl Congr. Applied Mechanics* (ed H. Görtler) pp1109-1115. Springer, Berlin, 1964.
11. Parmentier E.M. and C. Sotin, Three-dimensional numerical experiments on thermal convection in a very viscous fluid: Implications for the dynamics of a thermal boundary layer at high Rayleigh number, *Phys. Fluids* 12, 609-617, 2000.
12. Rhee, H., J. Koseff, and R. Street, Flow visualization of a recirculating flow by rheoscopic and liquid crystal techniques, *Exp. Fluids*, 2 , 57–64, 1984.
13. Chen F. and C.F. Chen. Experimental investigation of convective stability in a superposed fluid and porous layer when heated from below, *J. Fluid Mech.*, 207, 311-321, 1989.
14. Solomon, T., and J. Gollub, Thermal boundary layers and heat flux in turbulent convection: the role of recirculating flows, *Phys. Rev. A*, 43 , 6683–6693, 1991.
15. Gluckman, B., H. Willaime, and J. Gollub, Geometry of isothermal and isoconcentration surfaces in thermal turbulence, *Phys. Fluids A*, 5 , 647–651, 1993.
16. Moses E, Zocchi G and A. Libchaber, An experimental study of laminar plumes, *J. Fluid Mech.* 251 : 581—601, 1993.
17. Pottebaum, T.S., and M. Gharib, The pinch-off process in a starting buoyant plume, *Exp. Fluids*, 37 , 87-94, 2004.
18. Kimura, I., T. Hyodo, and M. Ozawa, Temperature and velocity measurement of 3D thermal flow using thermosensitive liquid crystals, *J. Visualization*, 1 , 145–152,1998.
19. Ciofalo, M., M. Signorino, and M. Simiano, Tomographic particle-image velocimetry and thermography in Rayleigh-Bénard convection using suspended thermochromic liquid crystals and digital image processing, *Exp. Fluids*, 34 , 156–172, 2003.
20. Fujisawa, N., and Y. Hashizume, An uncertainty analysis of temperature and velocity measured by a liquid crystal visualization technique, *Meas. Sci. Technol.*, 12 , 1235–1242, 2001.
21. Carslaw H. S. and J. C. Jaeger, *Conduction of heat in solids*, Oxford Clarendon Press, 1959.
22. Olson P. and H. Singer, Creeping plumes, *J. Fluid Mech.* 158 : 511—531, 1985.
23. Le Bars M. and A. Davaille, Large interface deformation in two-layer thermal convection of miscible viscous fluids, *J. Fluid Mechanics* 499 : 75—110, 2004
24. Davaille A and Vatteville J. On the transient nature of mantle plumes. *Geophys Res Lett*, 32, doi:10.1029/2005GL023029, 2005.
25. Solomatov S., Scaling of temperature- and stress-dependent viscosity convection. *Phys. Fluids*, 7: 266-274, 1995.

## Copyright Statement

The authors confirm that they, and/or their company or institution, hold copyright on all of the original material included in their paper. They also confirm they have obtained permission, from the copyright holder of any third party material included in their paper, to publish it as part of their paper. The authors grant full permission for the publication and distribution of their paper as part of the ISFV13/FLUVISU12 proceedings or as individual off-prints from the proceedings.